Lab on a Chip

Accepted Manuscript

ROYAL SOCIETY OF CHEMISTRY

www.rsc.org/loc

Lab on a Chip

RSCPublishing

ARTICLE

Electrical Cell-substrate Impedance Sensing with field-effect transistors is able to unravel cellular adhesion and detachment processes on a single cell level

Cite this: DOI: 10.1039/x0xx00000x

Received 00th April 2014,
Accepted 00th ??? 2014

DOI: 10.1039/x0xx00000x

www.rsc.org/

A. Susloparova,[a] D. Koppenhöfer,[a] J. K. Y. Law,[a] X. T. Vu[a] and S. Ingebrandt[a]

We introduce a novel technique of impedimetric sensing of cellular adhesion, which might have the potential to supplement the well-known technique of Electrical Cell-substrate Impedance Sensing (ECIS) in cell culture assays. In contrast to the already commercialized ECIS method, we are using ion-sensitive field-effect transistor (ISFET) devices. The standard gold microelectrode size in ECIS is in the range of 100-250 µm in diameter. Reason for this limitation is that when downscaling the sensing electrodes, their effective impedance governed by the metal-liquid interface impedance is becoming very large and hence the currents to be measured are becoming very small reaching the limit of standard instrumentation. This is the main reason why typical assays with ECIS are focusing on applications like cell-cell junctions in confluent cultures. Single cell resolution is barely reachable with these systems. Here we use impedance spectroscopy with ISFET devices having gate dimensions of only 16×2 µm^2, which is enabling a real single cell resolution. We introduce an electrically equivalent circuit model, explain the measured effects upon single cell detachment, and present different cellular detachment scenarios. Our approach might supplement the field of ECIS with an alternative tool opening up a route for novel cell-substrate impedance sensing assays with so far unreachable lateral resolution.

Introduction

Cellular morphology and cell-substrate adhesion strength are very important measures in different in vitro assays to evaluate and interpret the viability and the quality state of the cell culture under test.[1] Usually morphology evaluation is done by experienced cell biologists using phase-contrast microscopy. The cell-substrate adhesion provides the basis for different cellular functions like cell growth, proliferation and migration. In more detail, the cell-substrate adhesion can for instance be assessed on glass substrates by total internal reflection fluorescence (TIRF) microscopy.[2] The distance of the cellular membrane from the surface of the substrate can be assessed by fluorescence interference contrast microscopy on reflective substrates such as silicon.[3, 4] In literature other non-electrical methods utilizing microbalances have been presented as well.[5] An alternative and high-throughput method to evaluate the cell-substrate adhesion is electrical impedance spectroscopy. This technique of Electrical Cell-substrate Impedance Sensing (ECIS) is known for decades[6–10] and to date several systems are commercially available and applied in biomedical and pharmaceutical research.[11–13] In addition, complete cell culture analysis systems including metabolic monitoring are available.[14] However, these systems cannot provide single cell resolution. The minimum sizes of the metal electrodes for impedance monitoring in all these systems vary from 25 µm to 250 µm in diameter.[13] Typical cellular assays in ECIS are performed with epithelial cell lines forming complete, dense layers on the electrode structures. The ECIS method is then capable of recording changes in cell-cell junction, in membrane capacitance and sealing resistance of the cell-surface contact. For interpretation of ECIS data a model circuit has been established and used by researchers.[10] In more recent works the lateral limitation of the ECIS method has been described,[15] contact models for non-confluent tissue and a few individual cells on ECIS electrodes developed,[16] and several attempts for optimizing electrode design and passivation were made.[17, 18] The bottom line of all these studies is that generally the lower size limit for metal electrodes in bioimpedance assays is 50 µm in diameter.[18] Main limitation in ECIS is when downscaling the metal electrodes, the double layer capacitance formed at the metal-liquid interface is dominating the overall impedance of

the system and in this case cable impedance is playing a significant role.[19] All the above-mentioned studies conclude in general, that single cell resolution in ECIS assays is very difficult to reach, if not impossible to realize in a reliable manner.

Here we introduce an alternative method for ECIS using open-gate field-effect transistor (FET) devices. Open-gate FET devices have been widely used in the field of bioelectronics over past few decades.[20] They have been utilized for the detection of DNA sequences,[21, 22] action potentials of neuronal and cardiac cells,[23–25] and enzyme attachment and activities.[26, 27] A good overview of FETs used in cell culture assays is provided elsewhere.[28] Impedance spectroscopy with FETs is known for many years as well and has been applied to test the encapsulation of ISFET devices,[29] for immunosensing assays,[30] for protein detection,[27, 31] for DNA detection,[32] and for impedimetric sensing of cell-substrate adhesion. [33] In our recent studies, FET devices were used to detect the adhesion of individual cells[34] and to time-dependently access the effect of cytotoxic nanoparticles applied to the cultures.[35] In these former works, we presented the FET impedance data qualitatively comparing spectra with or without cells attached to the gate of the FETs or we presented time-dependent data recorded at a fixed frequency.[33]

In this article we focus on single cell assays and propose a model to interpret the recorded impedance spectra. An electrically equivalent circuit (EEC) for this liquid-solid junction is applied, which describes an FET device in contact with an adhered cell. This model is based on the so-called point-contact model, which is usually used to describe signal shapes of recorded action potential shapes of electrogenic cells.[36] To fully describe the spectral shape of our recordings we additionally need to include the parasitic values of the devices' feed lines and the frequency bandwidth of the transimpedance amplifier. In order to be able to fit the spectra and to extract the cell-related parameters, we derived an analytical solution for the EEC and fitted this equation to the measurement data using the software Origin (OriginPro 9.0, OriginLab Corporation, Germany). Our model takes variations of the seal resistance R_{seal} formed between the cellular membrane and the device surface and dynamic changes of the cellular shape, resulting in different values of the projected membrane capacitance C_M, into account.

Experimental

FET devices

We used p-channel, open-gate FET devices for the experiments presented in this study. The fabrication process of the FET devices was previously described.[18, 19] The devices were fabricated at the Institute for Microtechnique Mainz, Germany, during a former project at the Max-Planck Institute for Polymer Research Mainz, Germany. Sixteen transistor gates were arranged in a 4×4 array with a pitch of 200 µm in the center of a 5×5 mm^2 silicon chip. The gate dimensions were 16 µm in width and 5 µm in length and the thickness of the gate oxide was 8 nm. Chips were encapsulated at the University of Applied Sciences Kaiserslautern in Zweibrücken, Germany, by a modified, previously-described protocol.[18, 19] Chips were glued to a 28 DIL ceramic chip carrier (Global chip materials, LLC, Germany) and wire bonded. The electronic contacts were covered by PDMS (Sylgard 96-083, Dow Corning, Germany) and a glass ring (2.8 mm in diameter) was glued onto the chip for cell culture experiments.

Chip cleaning and surface modification

Before usage in a cell culture, the FET devices were cleaned and their surfaces were activated.[19, 20] Our FET devices are robust and can be re-used many times. The cleaning procedure includes the removing of the residues of the previous cell culture from the chip surface with ethanol and subsequent cleaning in two-steps of ultrasonic agitation (5 min in 2% Helmanex II (Hellma Analytics, Germany) and 5 min in distilled water). Afterwards the chip surfaces were activated for 30 min by 20% H_2SO_4 at 80 °C, subsequently rinsed with distilled water, and kept for 5 min in 70% ethanol for sterilization. Each FET surface was coated with 10 µl of 1 mg/ml fibronectin (AppliChem GmbH, Germany) and incubated at 37 °C for 3 hours. Before plating the cells, the surfaces were rinsed with distilled water.

Cell culture, drug treatment and chemicals

Two different cell lines, the human lung adenocarcinoma epithelial cell line H441 and the Human Embryonic Kidney HEK293 cell line, were used in this study. The H441 cells were grown in Roswell Park Memorial Institute medium (RPMI1640) supplemented with 1% L-Glutamine, 10% Fetal Calf Serum (FCS) and 1% Penicillin/Streptomycin while the HEK293 cells were grown in standard Minimal Essential Medium (M10) supplemented with 10% FCS, 1% Non-Essential Amino Acid (NEAA), 1% Penicillin/Streptomycin and 1% L-Glutamine. All chemicals were purchased from PAN Biotech GmbH, Germany. For the single cell experiments, a very low density of cells (3000 cells per FET device) was plated onto the device surface (2.8 mm in diameter). After 1 h of initial adherence, the chips were filled up with 200 µl of culture medium. All cell cultures were kept in an incubator at 37 °C with 5% CO_2. The measurements were typically performed after one day in vitro (DIV).

In order to induce detachment of the cells, trypsin (PAN Biotech GmbH, Germany) with a concentration of 5 µg/ml was used. For a second experiment this was lowered to 1 µg/ml in order to achieve a slower detachment process.

For drug-related experiments, cultured cells were treated with the apoptosis-inducing chemotherapeutic drug topotecan hydrochloride (Sigma-Aldrich, St. Louis, Missouri, USA). To induce apoptosis of the cells, 200 µl of culture medium were exchanged by 200 µl of drug containing medium with a concentration of 10 µg/ml.

Experimental setups

In this study we used two different amplifier setups, which were both previously described:

Transistor-transfer function (TTF) amplifier system

The TTF amplifier system was already described in previous works.[32, 33] This portable, 16-channel amplifier system was used to characterize the FET devices and to measure the frequency-dependent transfer functions. The custom-made system is based on a phase-selective amplifier system composed of a Direct Digital Synthesis (DDS) device and a multiplier followed by a low pass filter for all 16 channels in parallel. During the recording of the frequency spectra, the time constants of the amplifier are switched, which leads to smooth spectra from 1 Hz to 1 MHz.

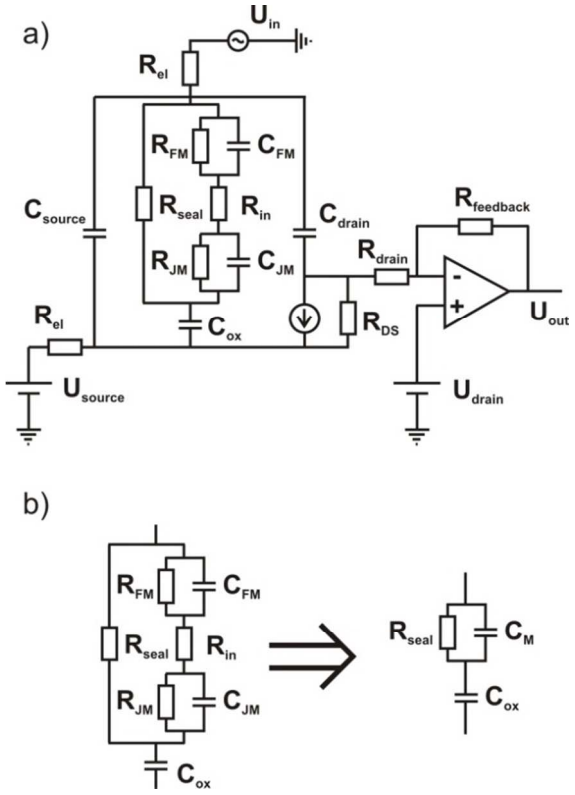

Fig 1 (a) An electrically equivalent electronic circuit, which describes a FET device in contact with an adherent cell on top of the transistor gate. All elements of the circuit are described in the text. (b) The cell-device interface part of the complete EEC is shown. The cell membrane is divided into a free (C_{FM}, R_{FM}) and a cellular junction part (C_{JM}, R_{JM}). In a first approximation this part can be simplified into only two elements C_M and R_{seal}., which are subsequently discussed as the cell-related parameters.

However, for precise fitting and interpretation of the data this circuit is difficult to interpret. The transfer functions were measured with this system by applying a sine signal with 10 mV amplitude and varying frequency. Time-dependent data can either be recorded in potentiometric or impedimetric mode by selection of a fixed frequency for phase-selective recording. All measurements can be controlled by means of read-out software implemented in Delphi 5.0 (Borland Software Corporation).

Lock-in amplifier setup

The experimental setup including a fast lock-in amplifier was previously described as well.[34] Figure 1S (in the supplementary material) shows a schematic diagram of this setup. A preamplifier for the FETs was connected to a fast lock-in amplifier (HF2LI, Zürich Instruments, Switzerland). This lock-in amplifier provides two high-frequency inputs and two analogue outputs. Using one of the analogue outputs, it was possible to apply a sinusoidal signal to the reference electrode, which was immersed into the electrolyte solution at a fixed position.

Main difference of the spectra recorded with one or the other setup are the high-pass characteristics at low frequency levels and the expanded high frequency range of the TTF setup. In case of the TTF amplifier the low pass effect is smoothened (see Figs. 2, 6a), whereas in the case of the lock- in amplifier setup this effect is clearly visible (see Figs. 5b, 6c, 6d, and 7d).

The drain-source and gate-source voltages of the FET devices were controlled via the analogue outputs of a data acquisition card (USB 6251, National Instruments, Inc). With this setup, it was possible to characterize the FET devices, to measure the frequency-dependent transfer functions, and to record time-dependent data at multiple frequencies. In comparison to the formerly used amplifier system,[32, 33] this new system has the following advantages: The bandwidth of the readout system is increased and the impedance spectra can be measured at higher frequencies (up to 50 MHz). The measured transfer functions are represented as bode plots including the complete amplitude and phase information. In addition, time-dependent readout can be achieved with the HF2LI system at several different frequencies, simultaneously. Since each analogue input of the lock-in amplifier can record data at three different frequencies, the recording of the time-dependent data was possible at six different frequencies for one channel or at three different frequencies for two channels, respectively.

Results and Discussion

Electrically equivalent circuit model of the cell-transistor contact

In a previous report we already presented an EEC model (Figure 1a), which describes an FET device in contact with an adherent cell.[34] Typically, the passive components of a cellular membrane can be described by the membrane capacitance and the membrane resistance in a parallel configuration. In similar cell-sensor contact models for interpretation of extracellular recorded action potentials the cell membrane is typically divided into a free part (C_{FM}, R_{FM}) and a part in the cellular junction (C_{JM}, R_{JM}).[37, 38] In a complete circuit, both elements should be connected by an inner resistance R_{in} of the cell's interior. The electrolyte-filled cleft of the junction area between cell and sensor is forming a resistive path, which is represented by the so-called seal resistance R_{seal}. This circuit part is in contact with a potentiometric sensor, i.e. the FET gate, where typically no resistive current is allowed into the device.[37, 38] In a first approximation this can be modelled by the gate oxide

capacitance C_{ox}. This part of the complete EEC is shown in the schematics in Figure 1b. Typical distance values between the cellular membrane and the transistor surface are in the range of several tens to 100 nm,[4, 39] which correspond to values of 0.5-2 MΩ for the seal resistance. It is therefore much smaller than the typical membrane resistances in the range of several GΩ.[37] Due to this fact the resistive path through the cell (R_{FM}, R_{in}, R_{JM}) can be neglected, such that the dominating resistive path in the contact area is represented by the seal resistance R_{seal} only. Therefore, the cell-FET contact can be condensed to a resistive part through the cell-sensor cleft (R_{seal}) and a capacitive part through the cell (C_M) with (Fig. 1b):

$$C_M = \frac{C_{FM} \cdot C_{JM}}{C_{FM} + C_{JM}} \quad (1)$$

This combined capacitance C_M should, however, should not be confused with the total membrane capacitance, which is typically measured by patch-clamp pipettes from inside to outside of a whole cell. Due to the serial combination of both membrane parts this combined membrane capacitance C_M is generally smaller than the typical whole-cell membrane capacitances of cells. Apart from these two cell-related parameters, the FET device parameters are strongly contributing to the complete transfer function of the system. The FET device can be described by the gate oxide capacitance C_{ox}, the transconductance g_m, and the output resistance R_{DS}. The parasitic parameters like contact line capacitances and series resistances of source and drain are contributing to the EEC with C_{source}, C_{drain}, and R_{source}, R_{drain}, respectively. The reference electrode and the electrolyte solution contribute in an ideal case only as resistive path to the circuit with a combined series resistance R_{el}. Due to the large number of elements this model is very complex and deriving an analytical solution for such an EEC is complicated.

In our experiments we measure the transfer function H (jω) for the signal transfer of a sinusoidal signal between the reference electrode input U_{in} (jω) and the signal output after the transimpedance amplifier stage U_{out} (jω) (Figure 1a).

$$H(jw) = \frac{U_{out}(jw)}{U_{in}(jw)} \quad (2)$$

By applying Kirchhoff's laws and considering rules for combination of impedances, an analytical equation representing the transfer function of our EEC model can be derived. The detailed derivation of this expression is presented in the supplementary material.

$$H(jw) = R_{feedback} g_m \cdot \frac{1}{\sqrt{1 + \left(\frac{f}{f_g}\right)^2}} \cdot \frac{1 + jw\left(C_M R_{seal} - \frac{C_L}{g_m}\right) - w^2 \frac{C_L R_{seal}}{g_m}(C_M + C_{ox})}{1 + jw(R_{seal}(C_{ox} + C_M) + R_{el}(C_L + C_{ox})) - w^2 R_{seal} R_{el}(C_L(C_{ox} + C_M) + C_{ox} C_M)} \quad (3)$$

In this equation several parameters need to be considered, which result in the typical shape of the measured transistor-transfer function (TTF) spectra. These parameters can be divided in chip-related parameters, transimpedance circuit parameters, and cell-related parameters:

- **Chip-related parameters:** FET transconductance g_m, gate oxide capacitance C_{ox}, contact line capacitance C_L, which is a parallel combination of the drain and source capacitances C_{drain} and C_{source}.
- **Transimpedance circuit parameters:** Series resistance of the reference electrode and electrolyte solution R_{el}, feedback resistance $R_{feedback}$ and cutoff frequency f_g of the operational amplifier
- **Cell-related parameters:** Combined membrane capacitance C_M and seal resistance R_{seal}

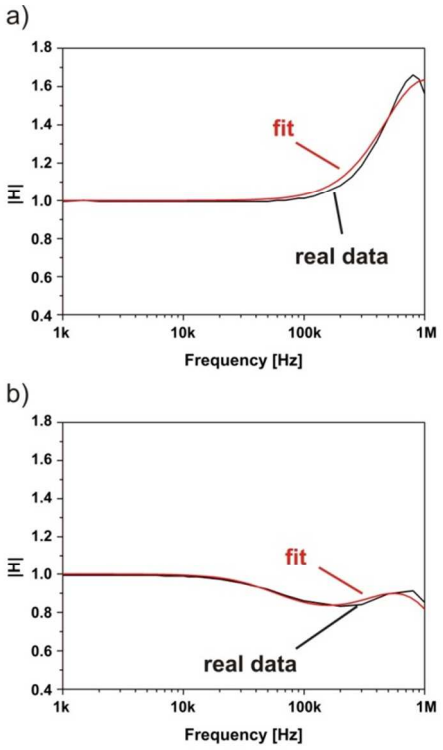

Fig 2 (a) Fit of a measured impedance spectrum for a cell-free transistor gate using equation 4. The values of the contact line capacitance and the FET transconductance are extracted to C_L = 92.2 pF ± 8.9 pF and g_m = 0.194 mS ± 0.015 mS, respectively. (b) Fit of a measured impedance spectrum for a cell-covered transistor gate using equation 3. The values of the seal resistance and the cell membrane capacitance are extracted to R_{seal} = 1.87 MΩ ± 0.15 MΩ and C_M = 1.21 pF ± 0.07 pF, respectively.

From equation 3 it can be seen that the relevant cell-related parameters are hidden inside a quite complicated expression. In our experiments we typically compare 'before' and 'after' measurements having either a cell attached to the FET gate or a completely free FET gate. Therefore, if the cell is completely detached, R_{seal} and C_M both become zero and equation 3 condenses to:

$$H(jw) = R_{feedback} g_m \frac{1-jw\frac{C_L}{g_m}}{1+jwR_{el}(C_L+C_{ox})} \frac{1}{\sqrt{1+\left(\frac{f}{f_g}\right)^2}} \quad (4)$$

Using these two equations we can obtain the cell-related parameters from our experiments by a comparison of the spectra with and without cell.

Fitting procedure for a cell-transistor contact using the EEC

In the following this will be demonstrated with an exemplary experiment presented in Fig. 2.

Using equation 4, the measured TTF-spectra without an adherent cell can be fitted and some parameters of the EEC in this particular experiment can be estimated. To start the fitting procedure with realistic start values, some of the chip-related parameters like the parasitic capacitances of source and drain contact lines C_{drain} and C_{source} and the gate oxide capacitance C_{ox} can be estimated from the simple plate capacitor equation:

$$C_{source/drain} = \frac{\varepsilon_0 \varepsilon_{ox} A_{source/drain}}{d} \quad (5)$$

, where ε_0 is the absolute permittivity of the vacuum (ε_0 = 8.8542·10^{-12} As/Vm), ε_{ox} is relative permittivity of silicon dioxide (ε_{ox} = 3.8), $A_{source/drain}$ is the area of the source or drain contact lines, and d is the respective thickness of the passivation layer, which are known from the fabrication process of the devices. In a similar manner the gate oxide capacitance can be estimated by:

$$C_{ox} = \frac{\varepsilon \varepsilon_0 WL}{d_{ox}} \quad (6)$$

, where W is the gate width, L is the gate length and d_{ox} is the thickness of the silicon oxide gate dielectrics. For our FET sensors with gate area of 16×2 µm^2 this results in 0.03 pF.

In a real experiment, these values can alternatively be derived from the FET electronic characteristics as well. For example the transconductance value g_m of the FET device in its working point is usually known from the device characterization prior to each experiment. In the TTF-spectra presented in Figure 2 the value of the series resistance R_{el} was estimated to 1 kΩ. The cutoff frequency f_g of the amplifier stage depends on the operational amplifier, which is used in the transimpedance circuit and on the value of the feedback resistor $R_{feedback}$ in the feedback loop. In our circuit we used the operational amplifier OP97 (Distrelec Schuricht GmbH, Germany) and a feedback resistor of $R_{feedback}$ = 10 kΩ, which resulted in a value for f_g of 750 kΩ. Using these start values in equation 4 the exemplary TTF-spectrum measured for a cell-free transistor can be fitted (Fig 2a). Out of this, two chip-related parameters namely the contact line capacitance C_L = 92.2 pF ± 8.9 pF and the transconductance g_m = 0.194 mS ± 0.015 mS were obtained (error ranges are resulting from the fitting procedure).

With this set of chip-related and circuit-related parameters, now the exemplary TTF-spectrum of the same transistor covered with one HEK293 cell can be fitted. As it can be seen in the graph, the measured data and fitted curves are in good agreement. Thereby, the cell-related parameters (C_M and R_{seal}) for this particular cell can be obtained. The fitted values of the seal resistance R_{seal} = 1.87 MΩ ± 0.15 MΩ and the cell membrane capacitance C_M = 1.21 pF ± 0.07 pF are in the expected range.[37] Such a combination of R_{seal} and C_M is characteristic for each cell-transistor contact and will vary with adhesion strength and cell shape, respectively.

Varying the cell-related circuit elements in the ECC model

Now that we have a good model for the TTF-spectra in hand, we can systematically study the influence of the cell-related parameters in two idealized scenarios. Typical values for the chip-related and transimpedance circuit parameters used for all simulations in the following are displayed in Table 1, while the cell-related parameters R_{seal} and C_M were varied in a wide range.

R_{el} [kΩ]	C_{sourc} [pF]	C_{drain} [pF]	R_{source} [Ω]	R_{drain} [Ω]	f_g [kΩ]
2	51	19	230	145	750

Table 1. The values of the elements contribute to the EEC circuit.

Influence of the seal resistance R_{seal}

In Figure 3 an idealized cell detachment process from the transistor surface is shown where the cell doesn't change its shape during detachment and is lifted up, stepwise. The gradual decrease of the seal resistance R_{seal} is exclusively related to an increase of the cleft height between the cell and the transistor surface. Figure 3 shows the simulated TTF-spectra varying R_{seal} in a range from 1 MΩ to 400 kΩ.

Step no.	h [nm]	R_{seal} [kΩ]
1	35	1051
2	50	735
3	70	525
4	90	408

Table 2. The seal resistance values depend directly on the cleft height. Values were calculated using equation 7.

In a previous publication of our group, an analytical equation for the value of the seal resistance R_{seal} for the case of a cell-transistor coupling experiment including an ionic current in the cleft carried by potassium ions was derived:[40]

$$R_{seal} = \frac{k_B T}{4\pi e_0^2 n_{tot}^B D_{K^+} h}\left[1 + 4\frac{L_D^2}{r^2}\left(\frac{1}{I_0(r/L_D)} - 1\right)\right] \quad (7)$$

, where k_B is the Boltzmann constant, T is the temperature, e_0^2 is the elementary charge, n_{tot}^B is a particle density of the surrounding bath solution, D_{K^+} is the diffusion coefficient of potassium in this former publication, h is the cleft height, I_0 is

the modified Bessel function, r is the cell radius, and L_D is the Debye length. For the values calculated in table 2, we assumed bulk conductivity in the cell-surface adhesion cleft as formerly described as 'bulk resistivity in cell adhesion'' (BRICA)-theory.[41] With this assumption, the measured R_{seal} values can be related to the average distance between cell membrane and device surface, which provides researchers with useful information about cell-substrate adhesion strength.

In order to apply this equation to our EEC for the interpretation of the TTF-spectra, we would need to consider the ionic strength of the electrolyte solution, which will result in a different value of n_{tot}^{B} and a global diffusion coefficient D for all ions carrying the test signal. In a first approximation the second term in the brackets of equation 7 can be neglected. In this case the seal resistance R_{seal} depends on the cleft height h, which is typically less than 100 nm for this cell type.[4, 39]

As it can be seen in figure 3b, the increase of the seal resistance is leading to a regular increase of the signal amplitude in the frequency range between 20 and 200 kHz, while the complete removal of the cell can be clearly distinguished.

Influence of the combined membrane capacitance C_M:

Changes in the combined membrane capacitance C_M can be estimated by simple geometrical considerations. This has been described for HEK293 before and the amount of membrane area attached to the surface was reported to lie in the range of 30-45% depending on the coating material used.[41] In this study here, we modelled an adherent cell as a hemisphere and a gradually detaching cell from the transistor surface with different spherical caps keeping the total surface area of the cell membrane constant (Figure 4).

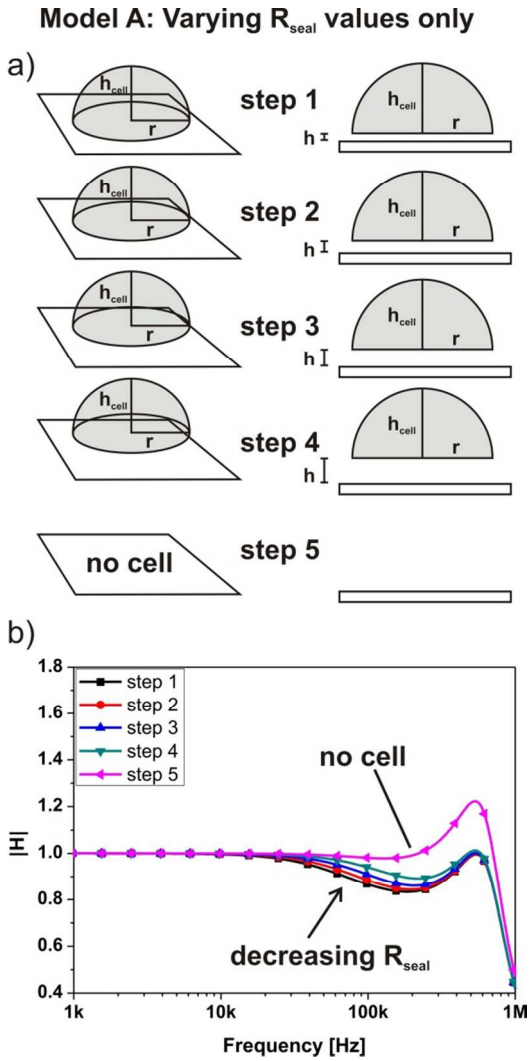

Fig 3 (a) Modelling of the cell detachment from the transistor surface in an idealized case where the cell doesn't change its shape during the detachment process. Only the cleft height h is increased stepwise resulting in the resistance values according to the values given in table 1. (b) The simulated TTF-spectra by varying of the seal resistance in a wide range (from 1 MΩ to 400 kΩ).

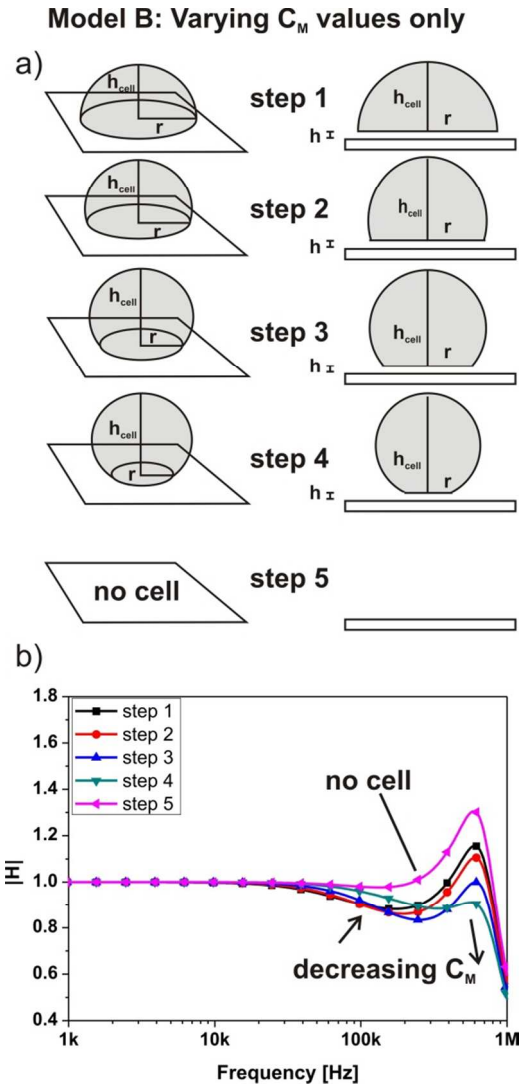

Fig 4 (a) Model of an adherent cell to the transistor surface and the gradually detached cell by simple geometrical shapes: The model excludes eventual shrinking or swelling effects of the cell since the overall surface area of the cell membrane is conserved in each step. The calculated capacitance values of the free and the attached cell at each step are given in table 3. (b) Simulated TTF-spectra for cell-covered gate (step 1), gate with the gradually detached cell (steps 2-4) and for cell-free transistor gate (step 5) are shown in the graph.

Of course this simple model is neglecting eventual swelling of shrinking of the cell. The area of the attached membrane part can be calculated with:

$$A_{JM} = \pi r^2 \quad (8)$$

, where r is the radius of the flat disc attached to the surface. The area of the free membrane part can be calculated with:

$$A_{FM} = \pi\left(a^2 + {h_{cell}}^2\right) \quad (9)$$

, where a is the radius of the base of the cap and h_{cell} is the height of the cap. Table 3 summarizes the calculated capacitance values of the free and the attached membrane in each step.

Step no.	r [µm]	a [µm]	h_{cell} [µm]	A_{JM} [µm^2]	A_{FM} [µm^2]	C_{JM} [pF]	C_{FM} [pF]	C_M [pF]
1	10	10	10	314	628	3.14	6.28	2.09
2	7.5	7.5	13.7	176.63	765.38	1.77	7.65	1.44
3	5	5	15.8	78.5	863.5	0.79	8.64	0.72
4	2.5	2.5	19.9	19.63	922.38	0.19	9.22	0.19

Table 3. The capacitance values depend on the geometry of the cell.

The calculations were performed assuming that the diameter of the model cell is 20 µm, which is resulting in a total membrane surface of 942 µm^2. This value was kept constant for all detachment steps. The values for capacitance of the free and the attached membrane parts were calculated by using a specific membrane capacitance of 1 µF/cm^2.

$$C_{FM/JM} = 1\,\frac{\mu F}{cm^2} A_{FM/JM} \quad (10)$$

Figure 4 shows the simulated TTF-spectra for the gradually deformed cell. The stepwise smaller capacitance values C_M for the cell membranes are leading to smaller absolute values in the spectra, which is an opposite effect compared to the seal resistance decrease during attachment.

In the range of small values of the attached membrane part some notable effects can be seen in the simulation. When the combined membrane capacitance C_M is coming close to the input capacitance of the FET gate C_{ox} (estimated to 0.03 pF) a notable change of the capacitive effect can be seen (Fig. 4). With decreasing C_M values first the spectra at the higher frequency range have smaller amplitude values, which with even smaller C_M values this trend is reversed. As it can be seen below such effects can be observed in the real experimental data as well.

In real experiments, of course both cell-related parameters will never vary independently. Therefore a fit to the EEC circuit model should be taken into account in any case extracting a combination of C_M and R_{seal} at particular time point during the detachment process.

Mechanical removal of an individual cell from the FET gate:

In order to be able to directly compare cell-attached and cell-detached configurations and to confirm that the changes in the TTF-spectra are exclusively caused by the adhesion of one single cell attached to the FET gate, we mechanically removed the respective cells under test with patch-clamp pipettes. For these experiments, the FET devices were covered by HEK293 cells in a low density and first the TTF-spectra were recorded with the cell attached.

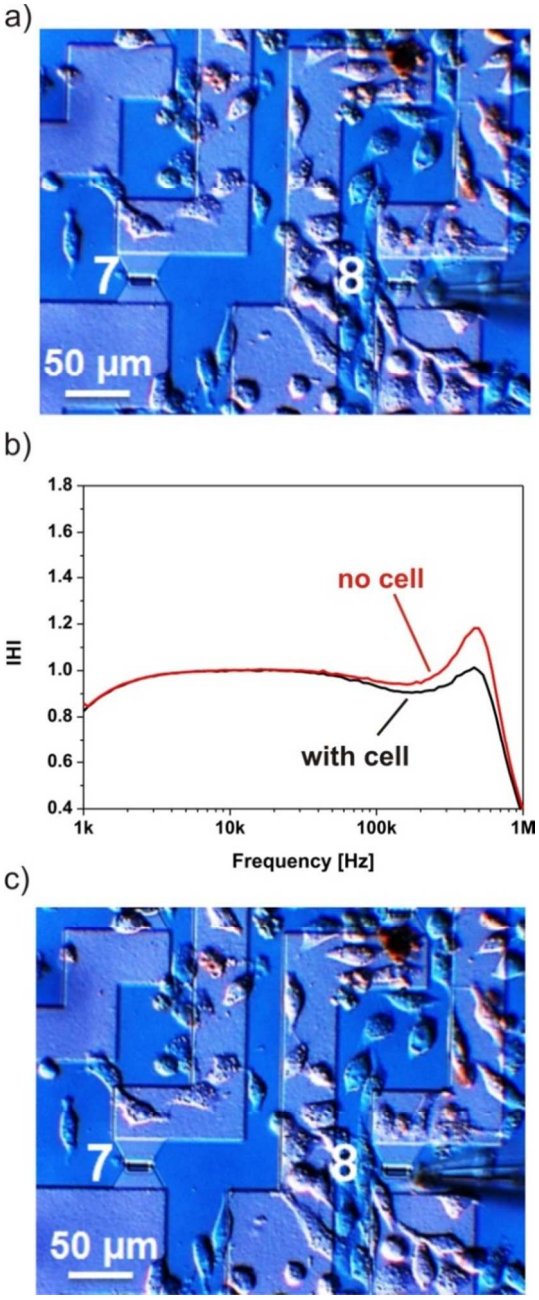

Fig 5 (a) Microscopic image of two transistor gates: Transistor gate 8 is covered by single HEK293 cell while transistor gate 7 is cell-free (b) Comparison of the TTF-spectra for the transistor gate 8 before and after removal of the single adhered cell with a patch-clamp pipette (c) Microscopic image after removal of the HEK293 cell from the transistor gate 8 with a patch-clamp pipette.

Figure 5 shows an exemplary experiment. Two transistor gates can be seen, with a single cell adhered to transistor gate number 8. This cell was removed by the patch-clamp pipette. The measured TTF-spectra before and after removal of the cell are compared in Figure 5. A significant change in the TTF-spectra shape can be observed. Using equation 3 the cell-related parameters of about C_M = 1.3 pF and R_{seal} = 604 kΩ can be extracted for the cell in this particular experiment.

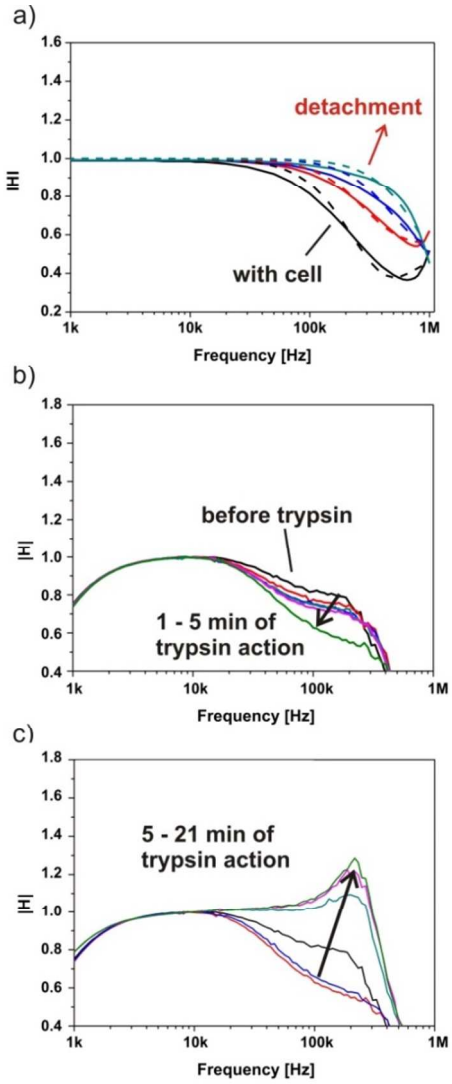

Fig 6 (a) Monitoring of the influence of the cell-related parameters on the TTF-shapes: The TTF spectra during the detachment process induced by 5 µg/ml trypsin solution were fitted and corresponding seal resistance and the cell membrane capacitance values are presented in Table 4 (Experiment 1). (b) The measured TTF spectra after adding of 1 µg/ml trypsin solution within the first 5 minutes. Measurement and saving of each TTF-spectrum required about 1 minute. A gradual decrease of the amplitude in the frequency range from 10 kHz to 400 kHz was observed. (c) In the second part of the cell detachment process the TTF-spectra showed an increase of the amplitude in the frequency range from 10 kHz to 400 kHz. Ten minutes after trypsin addition an optically visible morphology change was seen as well. The extracted parameters of the seal resistance and the cell membrane capacitance are presented in Table 4 (Experiment 2).

Chemical removal of cells from the FET chip:

In the initial experiments it was confirmed that the shape of the TTF-spectra is influenced by the cell-related parameters C_M and R_{seal} and stepwise changes are reflecting the gradually changing adhesion status of the cell.

To elucidate this, the chemically-induced detachment process of single cells was monitored while TTF-spectra were recorded stepwise. Two exemplary experiments are shown in the following. First, the HEK293 cells cultured in a low density on the FET device surfaces were treated with the 5 µg/ml trypsin protocol as described in the experimental section. Complete TTF-spectra were measured stepwise one after another within 5 min of cellular detachment. Changes in the shape of the TTF-spectra were clearly monitored (Figure 6a). This particular experiment was done with the TTF amplifier setup.

The measured TTF-spectra of these experiments were fitted incrementally using equation 3. The fitted values of the seal resistance R_{seal} and the cell membrane capacitance C_M for this experiment are presented in the Table 4 (experiment 1).

	R_{seal} [kΩ]	C_M [pF]
Experiment 1:		
before trypsin	1305 ± 45.2	0.21 ± 0.01
1 min after trypsin	540 ± 21	0.66 ± 0.02
2 min after trypsin	260 ± 11	0.62 ± 0.06
3 min after trypsin	135 ± 11	0.92 ± 0.07
Experiment 2:		
1 min after trypsin	1305 ± 81	0.15 ± 0.05
2 min after trypsin	1409 ± 110	0.18 ± 0.04
3 min after trypsin	1847 ± 167	0.27 ± 0.04
4 min after trypsin	2162 ± 202	0.29 ± 0.04
5 min after trypsin	3665 ± 278	0.23 ± 0.03

Table 4. The fitted values of the cell-related parameters like the seal resistance R_{seal} and the cell membrane capacitance C_M during the detachment process of the two experiments presented in Fig. 5.

Since this experiment was quite fast, we lowered the trypsin concentration to a value of 1 µg/ml. In some of these experiments we observed a different behaviour in the spectral shape changes. Measurement and saving of each TTF-spectrum required about 1 minute. These experiments were done with the lock-in amplifier setup. The complete measurement lasted for 21 min. The recorded TTF-spectra are shown in Figures 6b and 6c. As it can be seen, the cell-covered transistor gate responded immediately to the addition of trypsin with the gradually decrease in transfer-function amplitude in the frequency range from 10 kHz to 400 kHz (Figure 6b). After 10 minutes of the measurement, a gradual increase of the amplitude over time was monitored. After the complete measurement time of 21 min the typical shape for a cell-free transistor gate can be seen (Figure 6c). The optical control showed the morphological

changes of the cell from a flat to a round form. A combined effect of the seal resistance R_{seal} and the membrane capacitance C_M to the measured shape of the impedance spectra was clearly recognized (Table 4, experiment 2). In Table 4, experiment 2 the fitted values of the seal resistance R_{seal} and the membrane capacitance C_M for the first five measured TTF spectra are shown. In this period a gradual decrease in transfer-function amplitude was monitored (Figure 6b). Afterwards a gradual increase of the amplitude was monitored reversing the effect. This effect was similar to the experiment in Fig. 6a, which we attribute to a decrease of the seal resistance.

The first experiment was performed using TTF amplifier system which is comparable to the lock-in amplifier system has no high-pass effect. Therefore the measured TTF spectra for a cell-free transistor in Figure 6a and Figures 6b and 6c look different.

These two experiments represent typical recordings. In total 5 different cell culture weeks were recorded on several FET sensors having 16 channels. Many similar results and recordings were obtained. In another publication we present statistical evaluations of such single cell recordings.[43] In this publication here we discuss the model and pick individual measurements which are representative for such recordings.

The two typical recordings shown in figure 6 behave similar to the previously reported effects of trypsin and amphotericin B to HEK 293 cells.[33] In particular the recording shown in figure 6b, c was observed before. However, typically this is visible in time-dependent recordings at a fixed frequency, where such an inverse effect before complete detachment is visible as a 'dip' in the time trace.

This stronger adhesion can be interpreted according to our model to a stronger seal resistance and almost stable combined capacitance of the cell. It might be a hint towards the action of trypsin, which might digest the fibronectin coating or the extracellular matrix surrounding the cell leading to a time-limited stronger adherence prior to detachment. Nevertheless, we cannot fully exclude morphological effects. The reason is that our model presented here has some fundamental weaknesses.

It is generally known in the field of cell-sensor interface modelling, that the electrical contact is never a simple point contact. This is typically done by introducing area contact models, which would account for partly open FET areas and detachment effects in a inhomogeneous manner. In addition we exclude eventual swelling or shrinking effects.

Nevertheless comparable changes as in our recordings were observed on confluent cell layers using the ECIS approach and were regarded as morphological changes as onset of the cellular detachment process.[44]

Our model needs in future several refinements into these directions. We hope to read out of these spectra the fate of individual cell namely if the cell undergoes apoptosis or necrosis, which would be very valuable information for biomedical and pharmacological assays using our method of cell-substrate impedance sensing with field-effect transistor devices.

Time-dependent measurements using a chemotherapeutic drug: Finally, we present time-dependent experiments recording the apoptosis event induced by a chemotherapeutic drug. For these experiments H441 cells (papillary adenocarcinoma cell line) were cultured on the FET devices in a low density culture as well. The cells were then treated with the anti-cancer drug topotecan hydrochloride (10 µg/ml). Time-dependent measurements were performed 20 hours after drug administration. From earlier experiments, it was found, that the cells typically begin to respond roughly 20 hours after administration of the chemotherapeutic drug. Two transistor gates, one with a cell adhered to the gate surface (transistor gate 7 (Figure 7a)) and another cell-free gate (transistor gate 8 (Figure 7a)), were chosen to monitor the effect of topotecan on the H441 cells at two different frequencies within 4 hours, simultaneously. Since the cellular responses needed to be examined over a longer period, these measurements were performed inside an incubator at 37 ° C and 5% CO_2.

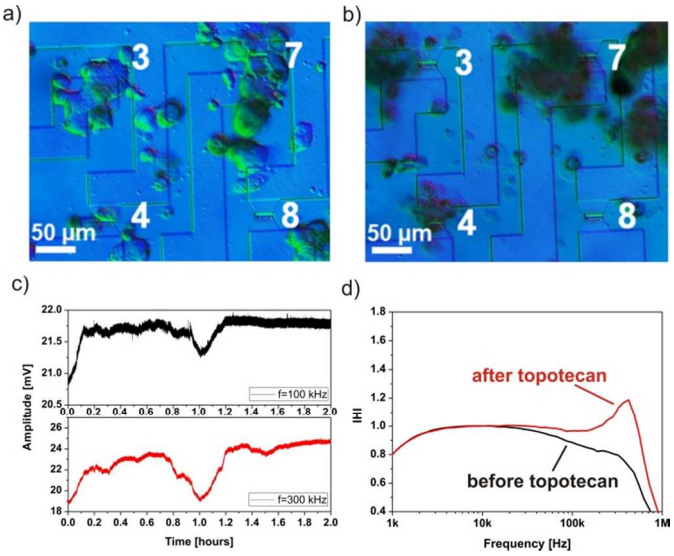

Fig 7 (a) Microscopic image of 4 out of 16 transistor gates covered by H441 cells: Gate 7 is cell-covered, while gates 3 and 4 are partially covered and gate 8 are cell-free. (b) The morphological changes induced after 24 hours of topotecan treatment. (c) Time-dependent measurement at two different frequencies (at 100 kHz and at 300 kHz) at the same time for a cell-covered transistor gate (gate 7). (d) Comparison of the TTF-spectra before and after 24 hours of topotecan (10 µg/ml) treatment (gate 7).

From the above discussions it is clear that the responses in the TTF-spectra may vary and that the time-course of the responses recorded at fixed frequencies are only fragmentary reflecting the changes in the cell-related parameters C_M and R_{seal}. When comparing the measured impedance spectra for a cell-covered and a cell-free transistor gate, it is obvious that the largest differences can be recorded in a frequency range from 30 kHz to 600 kHz. Two different frequencies in this range (100 kHz and 300 kHz) were chosen for the experiment. Figure 7c shows the measured amplitude over time at these two frequencies. Since the cells were completely detached after 2 hours, only this part of the recording is shown. The time evolutions of the measured curves at 100 kHz and 300 kHz are similar.

Comparable to the experiment presented in Figures 6, the amplitude of the transfer function firstly increased over time. After one hour the amplitude was dropping, which was more pronounced at the frequency of 300 kHz. Afterwards the amplitude of the transfer function increased again. A similar effect was observed by monitoring of the detachment process induced by trypsin solution, where the amplitude of the transfer-function was firstly decreased (Figure 6b) and afterwards increased again (Figure 6c). Such behaviour would lead to the typical dips, which we observed in our previous publications as well.[34, 35]

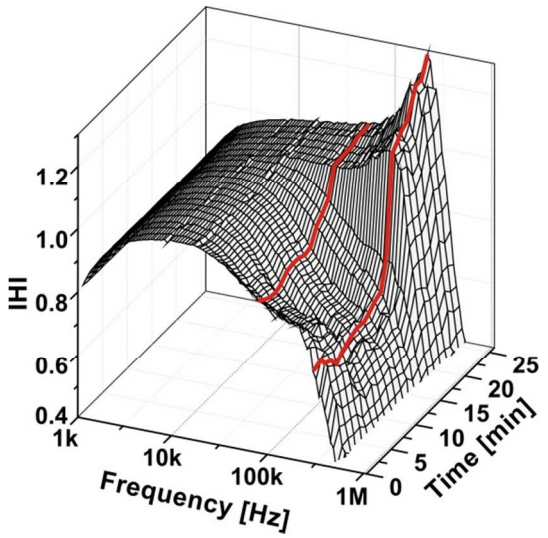

Fig 8 3D-representation of the time-dependent data shown in Fig. 6: Recording at fixed frequencies is not able to reveal detailed data of the detachment processes. Such time-dependent recordings (as shown in Fig. 7) can be understood as the red lines, which are exemplary drawn into the data. The shape of these lines is quite different. Only a full recording of the respective spectra with fitting to the EEC model can reveal the shape of the 3D landscape and can be used to interpret the cell-related parameters during cellular detachment.

From this experiment is obvious that a selection of only one fixed frequency, like it is usually done for some of the commercial ECIS systems,[12, 13] might mask important information and might lead to misinterpretation of the results. Only a complete frequency scan and a respective fit of the spectra can obtain the evolution of the cell-related parameters over time as it was previously described for the ECIS systems.[9, 43]

Similar to the ECIS data presented in these publications, we can as well represent our TTF-data in a 3-dimensional plot. The data of the stepwise experiment 2 shown in Figure 6b and c are displayed in Figure 8 as such a plot.

Exemplarily two lines were manually drawn into the 3-d landscape, which should underpin the reason for the differences typically observed in time-dependent measurements as described before and shown in Figure 7. Based on the simulation described above, we regard the gradual decrease of the amplitude in the TTF-spectra to a gradual increase of the seal resistor value (compare values in table 4). In a later part of the cellular detachment process the cell-matrix connections are broken and a gradual detachment of the cell is leading to a decrease of R_{seal} and consequently an increase of the TTF-amplitude. However, in time-dependent experiments at fixed frequencies such effects are very difficult to observe. We believe that in future recording always complete TTF-spectra should be recorded. A gradual fitting of the EEC while displaying C_M and R_{seal} values only, would allow following single cell adhesion detachment processes in detail. By this procedure eventually the individual cell fates could be distinguished. However, the design of such experiments remains unclear at the moment. It is very difficult to set up assays, where either apoptosis or necrosis could be fully excluded.

Conclusions and outlook

In this study, we demonstrated that by using FET sensors, impedimetric spectra of single cells attached to the substrate can be measured. It was clearly pointed out that the changes in the measured TTF-spectra are caused by the adhesion of individual cells on top of the FET gates. The measured TTF-spectra were interpreted by an EEC model composed of chip-related, transimpedance amplifier-related and cell-related parameters. Using this EEC model an analytical expression representing the transfer functions was derived, which was used to fit the measured impedance spectra and to extract the cell-related parameters of seal resistance and membrane capacitance. Also time-dependent readout at several different frequencies was recorded, simultaneously. However, such measurements are only partly reflecting the detachment process and time-dependent graphs are difficult to be explained.

Our proposed method of course also has some intrinsic shortcomings. When recording at the single cell level many sensors with many channels, fast data recording and sophisticated data analysis protocols would be needed. At the moment our method is still far from 'high-throughput' but we don't see fundamental limitations in this respect. In the current design we have a quite bulky reference electrode in the culture chamber, but eventually future chip designs could include chip-embedded reference electrodes. One major disadvantage for detailed interpretation is the use of the point contact model. We think that the extension towards area contact taking eventual effects of cell-free gate area into account would be beneficial. In addition for more realistic interpretation we would also need to allow for swelling and shrinking effects.

Nevertheless, our new method of individual cell impedance measurements with FET devices surely will add an additional tool to the field of impedance recording from cell cultures opening up the possibility of using non-confluent cell cultures in such assays. In contrast to the metal microelectrodes of the ECIS system, the FET devices can be reduced in lateral size. Compared to the ECIS method our devices have much smaller input impedance, since in the case of metal electrodes the main contribution is coming from the electrochemical double layer formed at the metal-liquid interface, while in the case of the FETs the gate dielectric layer is the main contribution to the input impedance. We previously discussed that for high resolution recordings, this input impedance should be as high as

possible. The lower impedance of FETs compared to the ECIS electrodes might be a disadvantage on a first glance, since then the cell-related changes are much better reflected in ECIS than in FET assays. However, when downscaling both approaches the higher impedances in ECIS turn into a disadvantage since then very small current modulations need to be recorded and transferred through the cables.[18] In contrast to this, the FET approach has a major advantage. The very small modulations of the gate voltage are directly converted by the devices itself and then transferred to through the cables on top of the constant drain-source currents, which are about 100× larger than this test signal. For instance in our devices the test signal of 10 mV recorded with a device having a transconductance of g_m = 0.2 mS is converted to a sinusoidal current of about 2 µA, which is carried through the cables as modulation on top of a constant drain-source current of about 0.7 mA. We believe that this is the main reason, why Electrical Cell-substrate Impedance Sensing with field-effect transistors can be downscaled to the single cell level.

Consequently, in future assays with our FET devices we will focus on such single cell experiments and on the further extension and refinement of the modelling of the spectra. In particular we want to use our approach to study other cell types like neurons. Eventually our method might find a commercial application. This novel FET-based ECIS (FETCIS) method might enable high resolution assays with non-confluent cell types like i.e. neurons or individually acting cells out of the immune system.

Acknowledgements

We thank the Federal Ministry of Education and Research (BMBF), Germany for financial support via the project "Entwicklung eines Zell-Chip Hybrid-Testsystems zur Wirksamkeitsanalyse von Krebsmedikamenten", 17008X10, and "Multifunktionales Pharmascreening mit Cell-Chip Hybridsystemen" ,17N2110.

Notes and references

[a] Department of Informatics and Microsystem Technology, University of Applied Sciences Kaiserslautern, Zweibrücken, 66482 (Germany)

Electronic Supplementary Information (ESI) available: We submitted a supplementary file for the complete derivation of equation 3. See DOI: 10.1039/b000000x/

1 T. Yeung, P. C. Georges, L. A. Flanagan, B. Marg, M. Ortiz, M. Funaki, N. Zahir, W. Ming, V. Weaver and P. A. Janmey, *Cell Motil. Cytoskeleton*, 2005, **60**, 24–34.

2 A. S. G. Curtis, *J. Cell Biol.*, 1964, **20**, 199–215.

3 A. Lambacher and P. Fromherz, *Appl. Phys. A Mater. Sci. Process.*, 1996, **63**, 207–216.

4 D. Braun and P. Fromherz, *Phys. Rev. Lett.*, 1998, **81**, 5241–5244.

5 K. A. Marx, Biomacromolecules, 2003, **4**, 1099-1120.

6 I. Giaever and C. R. Keese, *Proc. Natl. Acad. Sci. U. S. A.*, 1984, **81**, 3761–3764.

7 C. M. Lo, C. R. Keese and I. Giaever, *Biophys. J.*, 1995, **69**, 2800–2807.

8 I. Giaever and C. R. Keese, *Proc. Natl. Acad. Sci. U. S. A.*, 1991, **88**, 7896–7900.

9 J. Wegener, C. R. Keese and I. Giaever, *Exp. Cell Res.*, 2000, **259**, 158–166.

10 I. Giaever and C. R. Keese, *Nature*, 1993, **366**, 591–592.

11 AppliedBiophysics, "Applied Biophysics," can be found under http://www.biophysics.com/index.php, 2014.

12 ACEA Biosciences, "ACEA Biosciences -- xCELLigence System, Cell Index, E-Plate," can be found under http://www.aceabio.com/about.aspx, 2014.

13 Molecular Devices, "Molecular Devices," can be found under http://www.moleculardevices.com/, 2014.

14 Bionas Discovery 2500 system, "Bionas GmbH", can be found under http:// http://www.bionas-discovery.com/, 2014.

15 R. Pradhan, A. Mitra and S. Das, *Electroanalysis*, 2012, **24**, 2405–2414.

16 D. Mondal and C. RoyChaudhuri, *IEEE Trans. Nanobioscience*, 2013, **12**, 239–246.

17 D. T. Price, A. R. A. Rahman and S. Bhansali, *Biosens. Bioelectron.*, 2009, **24**, 2071–2076.

18 A. R. Abdur Rahman, D. T. Price and S. Bhansali, *Sensors Actuators, B Chem.*, 2007, **127**, 89–96.

19 C. Xiao, B. Lachance, G. Sunahara and J. H. T. Luong, *Anal. Chem.*, 2002, **74**, 1333–1339.

20 P. Bergveld, *Sensors Actuators B Chem.*, 2003, **88**, 1–20.

21 E. Souteyrand, J. P. Cloarec, J. R. Martin, C. Wilson, I. Lawrence, S. Mikkelsen, M. F. Lawrence, L. De Physicochimie, E. C. De Lyon and E. Cedex, *J Phys Chem B*, 1997, **5647**, 2980–2985.

22 F. Uslu, S. Ingebrandt, D. Mayer, S. Böcker-Meffert, M. Odenthal and A. Offenhäusser, *Biosens. Bioelectron.*, 2004, **19**, 1723–1731.

23 C. Sprössler, M. Denyer, S. Britland, W. Knoll and A. Offenhäusser, *Phys. Rev. E*, 1999, **60**, 2171–2176.

24 P. Fromherz, A. Offenhäusser, T. Vetter and J. Weis, *Science*, 1991, **252**, 1290–1293.

25 S. Ingebrandt, C. K. Yeung, M. Krause and A. Offenhäusser, *Biosens. Bioelectron.*, 2001, **16**, 565–70.

26 E. Katz and I. Willner, *Electroanalysis*, 2003, **15**, 913–947.

27 A. B. Kharitonov, J. Wasserman, E. Katz and I. Willner, *J. Phys. Chem. B*, 2001, **105**, 4205–4213.

28 A. Poghossian, S. Ingebrandt, A. Offenhäusser and M. J. Schöning, *Semin. Cell Dev. Biol.*, 2009, **20**, 41–48.

29 J. M. Chovelon, N. Jaffrezic-Renault, P. Clechet, Y. Cros, J. J. Fombon, M. I. Baraton and P. Quintard, *Sensors Actuators B Chem.*, 1991, **4**, 385–389.

30 R. B. M. Schasfoort, P. Bergveld, J. Bomer, R. P. H. Kooyman and J. Greve, *Sensors and Actuators*, 1989, **17**, 531–535.

31 J. Kruise, J. G. Rispens, P. Bergveld, F. J. B. Kremer, D. Starmans, J. R. Haak, J. Feijen and D. N. Reinhoudt, *Sensors Actuators B Chem.*, 1992, **6**, 101–105.

32 S. Ingebrandt, Y. Han, F. Nakamura, A. Poghossian, M. J. Schöning and A. Offenhäusser, *Biosens. Bioelectron.*, 2007, **22**, 2834–2840.

33 S. Schäfer, S. Eick, B. Hofmann, T. Dufaux, R. Stockmann, G. Wrobel, A. Offenhäusser and S. Ingebrandt, *Biosens. Bioelectron.*, 2009, **24**, 1201–1208.

34 A. Susloparova, D. Koppenhöfer, X. T. Vu, M. Weil and S. Ingebrandt, *Biosens. Bioelectron.*, 2013, **40**, 50–56.

35 D. Koppenhöfer, A. Susloparova, D. Docter, R. H. Stauber and S. Ingebrandt, *Biosens. Bioelectron.*, 2013, **40**, 89–95.
36 W. G. Regehr, J. Pine, C. S. Cohan, M. D. Mischke and D. W. Tank, *J. Neurosci. Methods*, 1989, **30**, 91–106.
37 S. Ingebrandt, C.-K. Yeung, M. Krause and A. Offenhäusser, *Eur. Biophys. J.*, 2005, **34**, 144–154.
38 R. Schätzthauer and P. Fromherz, *Eur. J. Neurosci.*, 1998, **10**, 1956–1962.
39 G. Wrobel, M. Höller, S. Ingebrandt, S. Dieluweit, F. Sommerhage, H. P. Bochem and A. Offenhäusser, *J. R. Soc. Interface*, 2008, **5**, 213–222.
40 M. Pabst, G. Wrobel, S. Ingebrandt, F. Sommerhage and A. Offenhäusser, *Eur. Phys. J. E. Soft Matter*, 2007, **24**, 1–8.
41 R. Gleixner and P. Fromherz, Biophysical Journal, 2006, 90, 2600-2611.
42 F. Sommerhage, R. Helpenstein, A. Rauf, G. Wrobel, A. Offenhäusser and S. Ingebrandt, *Biomaterials*, 2008, **29**, 3927–3935.
43 D. Koppenhöfer, F. Kettenbaum, A. Susloparova, J. K. Y. Law, X. T. Vu, T. Schwab, K. H. Schäfer, S. Ingebrandt, Biosens. Bioelectron., 2004, 10.1016/j.bios.2014.09.012
44 S. Arndt, J. Seebach, K. Psathaki, H.-J. Galla and J. Wegener, *Biosens. Bioelectron.*, 2004, **19**, 583–594.

